Catalysis Today xxx (xxxx) xxx–xxx

Contents lists available at ScienceDirect

Catalysis Today

journal homepage: www.elsevier.com/locate/cattod

# Hydrogen-generating behavior of Pd-decorated gold nanoparticles via formic acid decomposition

Zhun Zhao[a,1], Kimberly N. Heck[a,1], Pongsak Limpornpipat[a], Huifeng Qian[a], Jeffrey T. Miller[b], Michael S. Wong[a,c,d,e,*]

[a] Department of Chemical and Biomolecular Engineering, Rice University, 6100 S. Main Street, Houston, TX 77005, USA
[b] Davidson School of Chemical Engineering, Purdue University, West Lafayette, IN 47907, USA
[c] Department of Chemistry, Rice University, USA
[d] Department of Civil and Environmental Engineering, Rice University, USA
[e] Department of Materials Science and NanoEngineering, Rice University, USA

ARTICLE INFO

*Keywords:*
Nanoparticles
Palladium
Gold
Bimetallic
Formic acid
Hydrogen
Catalyst

ABSTRACT

Formic acid is a promising hydrogen storage material where hydrogen is generated via metal-catalyzed decomposition. Bimetallic catalysts are active for this reaction, but the mechanism has not been fully proven. Palladium metal supported on gold nanoparticles (Pd-on-Au NPs) has structural properties that are advantageous for studying aqueous-phase catalytic reactions. In this work, a series of Pd-on-Au NPs of varying Pd loadings (calculated in terms of Pd surface coverage, sc%) were synthesized, immobilized onto carbon, and studied for formic acid decomposition at room temperature. Pd-on-Au NPs were catalytically active, with a reaction rate constant as high as 137 m L-$H_2$/$g_{Pd}$/min (corresponding to an initial turnover frequency TOF of 123 $h^{-1}$) at a Pd loading of 300 sc%. In contrast, Au NPs were inactive, and Pd NPs were slightly active (5 mL-$H_2$/$g_{Pd}$/min and TOF of 38 $h^{-1}$). The Pd metal of Pd-on-Au catalysts are partially oxidized, and is readily reduced without changing the metal-on-metal structure during reaction, according to *in situ* x-ray adsorption spectroscopy measurements. CO formation was inhibited at a Pd loading of 300 sc%, suggesting that three-dimensional Pd ensembles favored the desired dehydrogenation pathway while single-atom and small two-dimensional Pd ensembles are active for the undesired dehydration pathway.

## 1. Introduction

The chemical energy per mass and zero carbon emissions of hydrogen makes it a very attractive potential energy carrier. However, its safe storage and transportation is problematic. Formic acid (HCOOH, "FA"), a liquid at room temperature, is a potential source for *in situ*-formed $H_2$ for fuel cells and hydrogenation reactions [1–3], due to its ability to decompose to form up to 4.4 wt% $H_2$. The decomposition of FA can occur through one of two exergonic reactions:

$$\text{Dehydrogenation: } HCOOH \leftrightarrow H_2 + CO_2 \Delta G = -48.4\ \text{kJ/mol} \quad \text{(R1)}$$

$$\text{Dehydration: } HCOOH \leftrightarrow H_2O + CO \Delta G = -28.5\ \text{kJ/mol} \quad \text{(R2)}$$

To produce continuous and stable $H_2$ flow at near-ambient conditions, reaction (1) is desired, whereas reaction (2) should be avoided since it consumes FA without $H_2$ generation and generates CO, a well-known fuel cell catalyst poison. Noble metals have been long been known to selectively catalyze FA dehydrogenation via reaction (1). These catalysts can be divided into two main categories: homogeneous metal-ligand complexes and supported metal catalysts. Homogeneous catalysts, based mainly on Ru, Ir, and Rh metals, have been shown to have excellent catalytic activities in FA decomposition at ambient temperature [4]. Catalyst recovery issues, use of ligands and solvents, and excessive additives limit their usefulness.

Monometallic Pd and Au catalysts have been both shown to exhibit some activity for the FA decomposition reactions, with some reports finding that PdAu bimetallic catalysts are more active than monometallics [5–10]. Catalysts were typically tested at high FA concentrations, under gas or liquid phase, and at elevated temperatures (> 50 °C). Many catalysts were shown to form high amounts of CO (10–1000 ppm), which likely contributes to catalyst deactivation.

Wang et al. observed that a graphene-supported Au@Pd (core@

* Corresponding author at: Department of Chemical and Biomolecular Engineering, Rice University, 6100 S. Main Street, Houston, TX 77005, USA.
*E-mail address:* mswong@rice.edu (M.S. Wong).
[1] These authors contributed equally to the manuscript.

https://doi.org/10.1016/j.cattod.2018.06.044
Received 20 December 2017; Received in revised form 5 June 2018; Accepted 28 June 2018
0920-5861/ 

shell) catalyst had greater activity compared to an alloyed AuPd catalyst, but the identity of the active site was not investigated [10]. Mullins and coworkers recently studied single-crystal model Au surfaces covered with various amounts of Pd, and found that the FA decomposition rate increased with increasing Pd loading up to 4 monolayers, and that $H_2$ production was maximized between 2–3 Pd monolayers [11]. It was proposed that Pd-metal centers were active for the initial decomposition reaction, and that interfacial Au was responsible for dehydration selectivity. This study was conducted in ultrahigh vacuum, far removed from the practical aqueous-phase conditions of $H_2$ generation from FA.

We suggest Pd-on-Au NP model catalysts (composed of Au NPs decorated with controlled amounts of Pd) can provide insights into FA decomposition chemistry. This bimetallic material is highly active for the aqueous phase hydrodechlorination (HDC) of chlorinated compounds [12–19], aqueous reduction of nitrite [20] and nitrophenol [21], as well as glycerol oxidation [22,23]. The activity of Pd-on-Au NPs is dependent on Pd content, which is quantified and metered by calculated Pd surface coverage (sc%), such that a "volcano-shaped" dependence of activity on Pd surface coverage was observed for the various reactions. Using X-ray absorption fine structure (XAFS) spectroscopy, we identified Pd surface species, ranging from single atoms to two-dimensional Pd ensembles (in which all Pd atoms are in contact with the Au) and three-dimensional Pd ensembles (in which a fraction of the Pd atoms do not contact the Au). Pd-on-Au NPs have a core-subshell structure where all Pd atoms are located on the surface of the Au-rich core and up to ~20% of them were oxidized, depending on surface coverage; monometallic Pd NPs had 25–35% of its Pd atoms as surface atoms and nearly all were oxidized [13,17,18]. Au NPs are essentially able to keep the surface Pd atoms in zerovalent form, leading to active sites that would not be present in Pd NPs under reaction conditions [17]. In this study, we synthesized carbon-supported Pd-on-Au NPs of a range of different Pd sc% and evaluated their catalysis for FA decomposition in a semi-batch reactor. The reaction products $CO_2$, CO, and $H_2$ were quantified, and selectivities were calculated. From *ex situ* and *in situ* XAS measurements of selected samples, bulk catalytic activity was correlated with Pd surface species, with the NPs with the highest Pd surface coverage as the most active and selective for FA dehydrogenation.

## 2. Experimental

### 2.1. Materials

Tetrachloroauric acid ($HAuCl_4{\cdot}3H_2O$, > 99%), tannic acid ($C_{76}H_{52}O_{46}$, > 99.5%), potassium carbonate ($K_2CO_3$, > 99.5%), palladium chloride ($PdCl_2$, 99.99%), formic acid (HCOOH, 98%), and activated carbon (Darco-G60) were purchased from Sigma-Aldrich. Sodium citrate dihydrate ($Na_3C_6H_5O_7{\cdot}2H_2O$, > 99.5%) was purchased from Fisher Scientific. Commercially available 1 wt% $Au/Al_2O_3$ was obtained from Mintek. Helium (99.99%), hydrogen (99.99%), carbon monoxide (99.99%), and carbon dioxide (99.99%) were purchased from Matheson. All experiments were conducted in Nanopure water (> 18 MΩ-cm, Barnstead NANOpure Diamond). All chemicals were used as received unless otherwise noted.

### 2.2. Catalyst preparation

All NPs were synthesized using well-developed protocols reported in our earlier studies (see Supporting Information) [24–26]. Four compositions representative of < 100 sc% and > 100 sc% NPs were chosen: 30 sc%, 60 sc%, 150 sc% and 300 sc% Pd-on-Au. The Pd loading for all Pd-on-Au/C catalysts was kept constant at 1 wt%, while the Au loading varied according to the calculated Pd surface coverage.

For the 30 sc% Pd-on-Au/C sample, 2.814 L of sol were mixed with 1 g of activated carbon. The mixture was stirred for ~24 h at 700 rpm, cooled to 4 °C, and centrifuged for 40 min at 14,000 rpm. The carbon slurry was collected and dried in a vacuum oven at 70 °C overnight until no further mass loss from evaporated water was observed. The material was then ground into powder form and stored in the dark at ambient conditions. Activated carbon, in the untreated ("as-is" carbon) and treated forms ("as-processed" carbon), were used in control experiments. 60, 150, 300 sc% Pd-on-Au/C samples were prepared similarly using 1407, 542, and 290 mL of sol. The resulting solids of 30, 60, 150, 300 sc% Pd-on-Au/C were calculated to have 13.5, 6.8, 2.5 and 1.4 wt% Au, respectively. Carbon-supported with 1 wt% Au (Au/C) was prepared in the same manner by mixing 204 mL of Au sol (49.7 mg Au/L) with 1.0 g of activated carbon; carbon-supported with 1 wt% Pd (Pd/C) was prepared in the same manner by mixing 314 mL of Pd sol (31.8 mg Pd/L) with 1.0 g of activated carbon.

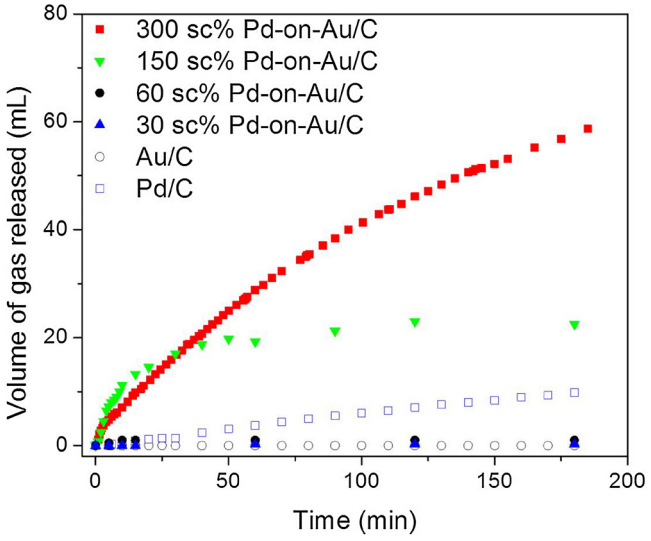


**Fig. 1.** Volume of gas released profile for Au/C, Pd/C, and 30, 60, 150 and 300 sc% Pd-on-Au/C catalysts. Reaction conditions: 0.5 g catalyst (1 wt% Pd with variable Au content), 23 °C, 1200 rpm stirring rate, 10 mL of 1 M formic acid.

### 2.3. Catalytic testing

Catalytic activity was evaluated in a homemade semi-batch reactor by measuring the gas release rate from the reactor (Scheme S1) at room temperature (23 ± 1 °C). 500 mg of catalyst powder was loaded into a glass vial (40 mL, VWR), which was then sealed with Teflon tape and a Teflon-coated rubber septum. The total Pd charge to the reactor was 125 mg-Pd/L-fluid for all Pd-containing catalysts. The reactor was first connected to a CO electrochemical detector (0–300 ppm with 0.1 ppm precision, Environmental Sensors Co.), and then connected with a horizontally laid plastic bottle (2 L, VWR) loaded with 1.8 L water (acidified to pH 4 to prevent $CO_2$ dissolution) in series. The amount of gas formed over time was quantified by weighing the amount of water displaced from the plastic bottle by the gaseous reaction products. A series of experiments varying the amount of the most active catalyst were conducted to ensure the reaction was not mass transfer limited [16,22] (see Supporting Information).

The composition of the gas phase products was analyzed by injecting 250 µL of headspace sample into an Agilent Technologies 6890 N gas chromatography (GC) equipped with a thermal conductivity detector (TCD) and a ResTek PC 3533 Hayesep Q. 60180 packed column. A GC method with a run time of 4.5 min, helium carrier gas at a flow rate of 10 mL/min, and an oven temperature of 35 °C was used. Standard curves for $H_2$, CO, and $CO_2$ were prepared by injecting various volumes of a gas standard (100 ppm CO, 49.995% $H_2$, 49.995% $CO_2$, Matheson, see Fig. S2 for representative chromatogram). CO content in ppm was directly read from the digital display of the CO electrochemical detector calibrated with known CO concentrations.

**Table 1**
Catalytic activity results for carbon-immobilized Au, Pd, and Pd-on-Au NPs. Reaction conditions: 0.5 g catalyst, 23 °C, 1200 rpm stirring rate, 10 mL, 1 M formic acid. Each reaction rate constant was the average of three runs.

| Catalyst type | Volume of gas released after 3 h (mL) | Initial $H_2$ generation rate (L $h^{-1}$ $g_{Pd}^{-1}$)[a] | $k_{cat}$[b] (L $g_{Pd}^{-1}$ $h^{-1}$) | Initial TOF mol-FA·mol-surface-$Pd^{-1}$·$h^{-1}$ | $H_2$:$CO_2$ molar ratio[c] | CO:$CO_2$ molar ratio[c] |
|---|---|---|---|---|---|---|
| $C_{received}$ | 0 | 0 | – | – | – | – |
| $C_{processed}$ | 0 | 0 | – | – | – | – |
| Au/C | 0 | 0 | – | – | – | – |
| 30 sc% | < 0.2 | | $1.6 \times 10^{-7}$ | $1.6 \times 10^{-9}$ | 0.99 | $1.03 \times 10^{-2}$ |
| 60 sc% | 1.0 | 0.06 | 0.024 | 2.6 | 1.0 | $3.01 \times 10^{-4}$ |
| 150 sc% | 22.5 | 7.98 | 0.162 | 35.2 | 1.0 | $6.86 \times 10^{-6}$ |
| 300 sc% | 58.2 | 8.22 | 0.157 | 123 | 1.0 | 0 |
| Pd/C | 9.8 | 0.30 | 0.043 | 38 | 1.0 | $3.70 \times 10^{-6}$ |

[a] Initial $H_2$ generation rate based on $H_2$ generation rate after 5 min reaction.
[b] First-order reaction rate constants were calculated using data points in the first 2 h. Reaction rate constants were calculated from the first 0.5 h of the concentration-time profile for Pd/C, and for the first 1 h of the concentration-time profile for 100, 150, and 300 sc% Pd-on-Au/C catalysts.
[c] After 20 min reaction time.

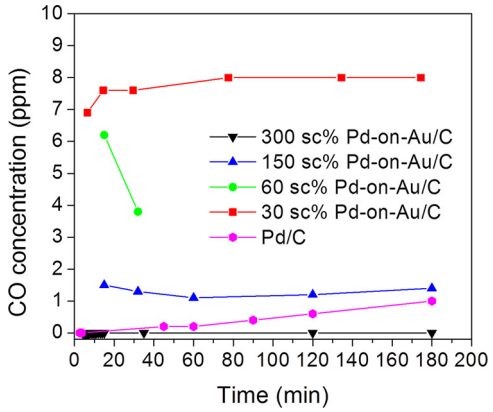


**Fig. 2.** CO concentration profiles for Au/C, Pd/C, and 30, 60, 150 and 300 sc% Pd-on-Au/C catalysts. Reaction conditions: 0.5 g catalyst, 23 °C, 1200 rpm stirring rate, 10 mL, 1 M formic acid.

At 23 °C, the molar volume for an ideal gas is 24.3 L/mol. Since the reaction generates equal volume amount of $CO_2$ and $H_2$, the converted amount of FA ($C_{FA,0}$-$C_{FA}$, where $C_{FA}$ and $C_{FA,0}$ were the time-dependent and initial formic acid concentrations (mol-FA $L^{-1}$) respectively) can be calculated as $V/(2 \times 24.3)$, where $V$ is the volume of the gas evolved in liters. Thus, $C_{FA}$ can be further expressed as:

$$C_{FA} = C_{FA,0} - \frac{V}{(2 \times 24.3)} \quad (1)$$

Formic acid decomposition reaction kinetics was modeled as a pseudo-first-order reaction (2) with respect to formic acid.

$$\frac{dC_{FA}}{dt} = k_{meas} C_{FA} \quad (2)$$

The apparent initial first-order reaction rate constant, $k_{meas}$ (with units of $h^{-1}$), was calculated from fitting Eq. (3) to the first 2 h of the concentration-time profiles, where $t$ is the reaction time. For catalysts observed with deactivation, $k_{meas}$ was also calculated by fitting Eq. (2) to the first 1 h of the concentration-time profiles as a comparison.

$$C_{FA} = C_{FA,0} e^{-k_{meas} t} \quad (3)$$

The metal-normalized rate constant $k_{cat}$ (with units of L $g_{Pd}^{-1}$ $h^{-1}$) was defined as $k_{meas}$ divided by the Pd metal content charged to the reactor ($C_{Pd}$, $g_{Pd}$ $L^{-1}$):

$$k_{cat} = \frac{k_{meas}}{C_{Pd}} \quad (4)$$

To represent catalytic activity at the particle surface, initial turnover frequency (TOF) was defined as

$$TOF = k_{meas} C_{FA,0} C_{sPd} \quad (5)$$

(with units of mol-FA mol-surface-$Pd^{-1}$ $h^{-1}$), where $C_{sPd}$ is the surface metal content (mol-surface-Pd $L^{-1}$) of the reactor, estimated using the magic cluster model [22] (see Supporting Information for details).

### 2.4. Ex situ and in situ X-ray absorption spectroscopy (XAS)

Catalyst samples were analyzed through both *ex situ* and *in situ* XAS modes. XAS measurements were carried out on Au $L_3$ (11.919 keV) or Pd K (24.350 keV) edges on the insertion device (beamline 10-ID-B) of the Materials Research Collaborative Access Team (MRCAT) at the Advanced Photon Source at Argonne National Laboratory. Detailed instrumentation can be found in our earlier studies [17,26,27].

*Ex situ* XAS spectra of each sample were collected first under air at room temperature. The samples were then treated under flowing 4% $H_2$/He gas for ~30 min at 200 °C and cooled to room temperature under a He purge. Based on our previous studies, this treatment method fully reduces oxidized Pd in the Pd-on-Au NPs without affecting the bimetallic nanostructure [17]. The reduced samples were then analyzed under He at room temperature to determine the extent of Pd oxidation in the Pd/C and Pd-on-Au/C samples.

*In situ* XAS measurements were taken using a liquid cell fabricated out of polyether ether ketone (PEEK) with Kapton windows. The cell was equipped with gas inlet-outlet and liquid injection ports, and was capped with a Swagelok VCR fitting with O-ring seal. Prior to measurement, the cell was loaded with 200 mg of catalyst and purged with He gas at 50 mL/min for 15 min. The gas inlet port was turned off and the outlet port was connected to a plastic tube immersed in water to avoid pressure build-up in the cell. The reaction was initiated by injecting 0.5 mL of 0.5 M formic acid solution through the injection port, and *in situ* XAS measurements were taken in transmission mode every 5 min for 30 min.

## 3. Results and discussion

### 3.1. Activity of Pd-on-Au NPs for formic acid decomposition

The activity of the catalysts for formic acid decomposition at room temperature was evaluated for monometallic Au, Pd, and bimetallic Pd-on-Au/C. Fig. 1 shows the volume of gas released versus time and Table 1 lists the calculated reaction rate constants.

The Au/C catalyst had no activity as no gas formation was observed after 3 h of reaction time (Fig. 1, Table 1), consistent with Sabatier and co-worker's observations that Au was the least active for this reaction

**Table 2**
*Ex situ* EXAFS fit parameters for catalysts.

| Catalyst | Treatment | Scattering Edge | Scattering path | CN ( ± 10%) | R, Å ( ± 0.02 Å) | DWF ($\times 10^3$ Å$^2$) | $E_o$ (eV) |
|---|---|---|---|---|---|---|---|
| Au/C | None | Au | Au-Au | 9.5 | 2.86 | 1.0 | −0.6 |
| | $H_2$ 200 °C | | Au-Au | 9.3 | 2.86 | 1.0 | −1.0 |
| Pd/C | None | Pd | Pd-O | 2.3 | 2.04 | 1.0 | −5.6 |
| | | | Pd-Pd | 3.5 | 2.74 | 1.0 | −1.0 |
| | $H_2$ 200 °C | | Pd-Pd | 8.6 | 2.75 | 1.0 | 0.2 |
| 60 sc% Pd-on-Au/C | None | Au | Au-Au | 9.1 | 2.85 | 0.0 | −0.4 |
| | | | Au-Pd | 2.3 | 2.78 | 0.0 | 2.6 |
| | | Pd | Pd-O | 0.9 | – | – | – |
| | | | Pd-Pd | 0.6 | 2.75 | 0.0 | 0.2 |
| | | | Pd-Au | 9.8 | 2.78 | 0.0 | −6.7 |
| | $H_2$ 200 °C | Au | Au-Au | 9.4 | 2.86 | 0.0 | 0.2 |
| | | | Au-Pd | 2.2 | 2.80 | 0.0 | 2.3 |
| | | Pd | Pd-Pd | 0.6 | 2.75 | 0.0 | 0.2 |
| | | | Pd-Au | 10.0 | 2.78 | 0.0 | −7.0 |
| 150 sc% Pd-on-Au/C | None | Au | Au-Au | 8.8 | 2.85 | 0.0 | 0.3 |
| | | | Au-Pd | 2.4 | 2.78 | 0.0 | 2.9 |
| | | Pd | Pd-O | 1.3 | 2.04 | 1.0 | 0.6 |
| | | | Pd-Pd | 1.5 | 2.75 | 1.0 | −3.9 |
| | | | Pd-Au | 7.3 | 2.78 | 1.0 | −6.0 |
| | $H_2$ 200 °C | Au | Au-Au | 8.7 | 2.85 | 0.0 | 0.9 |
| | | | Au-Pd | 2.5 | 2.78 | 0.0 | 2.9 |
| | | Pd | Pd-Pd | 2.0 | 2.75 | 1.0 | −2.0 |
| | | | Pd-Au | 7.8 | 2.78 | 1.0 | −5.8 |
| 300 sc% Pd-on-Au/C | None | Au | Au-Au | 8.6 | 2.85 | 0.0 | −0.6 |
| | | | Au-Pd | 2.4 | 2.78 | 0.0 | 4.8 |
| | | Pd | Pd-O | 2.6 | 2.04 | 1.0 | −1.3 |
| | | | Pd-Pd | 1.1 | 2.75 | 1.0 | 2.0 |
| | | | Pd-Au | 2.3 | 2.78 | 1.0 | −2.5 |
| | $H_2$ 200 °C | Au | Au-Au | 8.5 | 2.85 | 0.0 | 0.4 |
| | | | Au-Pd | 3.1 | 2.78 | 0.0 | 4.1 |
| | | Pd | Pd-Pd | 6.5 | 2.75 | 1.0 | 2.1 |
| | | | Pd-Au | 2.7 | 2.78 | 1.0 | −4.1 |

compared to other metals [28,29]. Bi et al. recently reported the very high activity of Au supported on $ZrO_2$ catalyst, which had a TOF of 1590 $h^{-1}$ at 50 °C for formic acid decomposition in triethylamine [30]. They concluded that reaction proceeds unimolecularly *via* an amine-assisted formate decomposition mechanism at the Au–$ZrO_2$ interface. Otherwise, Au generally has little activity [5–7].

Pd content increased catalytic activity (Fig. 1, Table 1). The 30 sc% Pd-on-Au NPs had a very small rate constant, with trace amounts of gas (< 0.2 mL after 3 h) were observed. The 60 sc% Pd-on-Au/C was slightly more active with ~1.0 mL gas released within 3 h, and had a calculated TOF value of 2.6 $h^{-1}$. The 150 sc% Pd-on-Au/C initially had a faster gas release during the first 10 min after which the release rate slowed down, with a total of 22.5 mL gas generated at 3 h. The TOF value of 150 sc% Pd-on-Au/C was calculated to be 35.2 $h^{-1}$, higher than the 60 sc% one by 13.5 times.

The 300 sc% Pd-on-Au/C was the most active catalyst, generating 58.2 mL of gas in 3 h and exhibiting no apparent deactivation. Compared with published results, our Pd-on-Au catalyst was much more active than other bimetallic PdAu catalysts (Table S1), and was in the range of homogeneous Ru catalysts with a TOF value of 123 $h^{-1}$.

### 3.2. Selectivity

The $CO_2$ to $H_2$ molar ratio was 1.00 ± 0.05 at all reaction times for all catalysts, consistent with the FA dehydrogenation pathway (Table 1). Dehydration was co-occuring to a limited extent, with ppm-level formation of CO for most Pd-containing catalysts (Fig. 2). Au/C was not active and did not generate any CO. Pd/C had an increasing amount of CO during reaction, reaching ~1 ppm after 3 h of reaction. The 30 sc% Pd-on-Au/C catalyst generated the most CO (~8 ppm) during the reaction. Increasing the Pd content to 60 sc% and 150 sc% Pd decreased the amount of CO generated to ~5 ppm and ~1 ppm, respectively.

The proportion of CO formed relative to $CO_2$ decreased with increasing Pd surface coverage, with 300 sc% Pd-on-Au/C (the most active catalyst) generating no detectable amount of CO. The trend in CO concentration is consistent with the observed activity order of the catalysts, correlating catalyst deactivation to the dehydration pathway (due to CO formation). This correlation of higher FA decomposition activity and lower CO formation suggests dehydrogenation dominates over dehydration with increasing Pd surface coverage (at which there are less PdAu interfaces and larger Pd ensembles). This observation agrees with what Tedsree et al. observed for Ag-Pd bimetallic NPs catalyzed room temperature formic acid decomposition [31], and those of Mullins and coworkers who suggested that PdAu interface sites are active for the dehydration pathway [11].

### 3.3. XAS structures of catalysts

The EXAFS fit parameters of the *ex situ* measurements of the catalysts are shown in Table 2. For the Au/C catalyst, a Au-Au coordination number (CN) of ~9.5 (Table 2) corresponds to an average NP size of ~4.3 nm based on TEM-EXAFS size correlation developed for supported Au materials [32]. Au atoms were all in metallic state with no evidence of oxidation, and no change was observed after treating with $H_2$. This result is consistent with our previous studies [17,22,26].

All catalysts containing Pd, however, did contain some oxidized Pd, which is likely due to handling and storage of the catalysts in ambient air. The 60 sc% Pd-on-Au/C had coordination numbers similar to our previous results [17,26], indicating a core-shell structure. A Pd-Pd CN value of 0.6 and Pd-O CN value of 0.9 indicated the Pd atoms were present as small 2-dimensional (2-D) ensembles and that ~20% of those atoms are oxidized. This untreated sample's *ex situ* result is similar to our previous results for 60 sc% Pd-on-Au NPs. [17,22]

Based on the high Au-Au CNs, the 150 sc% and 300 sc% Pd-on-Au/C catalysts also exhibited Au-core and Pd-shell structure, and had

**Table 3**
*In situ* EXAFS fit parameters for catalysts under reaction conditions: 0.2 g catalyst, 23 °C, 0.5 mL, 0.5 M formic acid.

| Catalyst | Time point | Scattering Edge | Scattering path | CN ( ± 10%) | R, Å ( ± 0.02 Å) | DWF ($\times 10^3$ Å$^2$) | $E_o$ (eV) |
|---|---|---|---|---|---|---|---|
| Au/C | Baseline | Au | Au-Au | 9.5 | 2.86 | 1.0 | −0.6 |
| | 5 min | | Au-Au | 9.3 | 2.86 | 1.0 | −0.3 |
| Pd/C | Baseline | Pd | Pd-O | 2.3 | 2.04 | 1.0 | −5.6 |
| | | | Pd-Pd | 3.5 | 2.74 | 1.0 | −1.0 |
| | 5 min | | Pd-O | – | – | – | – |
| | | | Pd-Pd | 7.3 | 2.76 | 1.0 | 0.1 |
| 60 sc% Pd-on-Au/C | Baseline | Au | Au-Au | 9.1 | 2.85 | 0.0 | −0.4 |
| | | | Au-Pd | 2.3 | 2.78 | 0.0 | 2.6 |
| | | Pd | Pd-O | 0.9 | – | – | – |
| | | | Pd-Pd | 0.6 | 2.75 | 0.0 | 0.2 |
| | | | Pd-Au | 9.8 | 2.78 | 0.0 | −6.7 |
| | 5 min | Au | Au-Au | 8.8 | 2.85 | 0.0 | −0.3 |
| | | | Au-Pd | 2.4 | 2.78 | 0.0 | 3.1 |
| | | Pd | Pd-O | 0.9 | – | – | – |
| | | | Pd-Pd | 0.4 | 2.75 | 1.0 | 0.2 |
| | | | Pd-Au | 9.5 | 2.78 | 1.0 | −7.3 |
| 150 sc% Pd-on-Au/C | Baseline | Au | Au-Au | 8.8 | 2.85 | 0.0 | 0.3 |
| | | | Au-Pd | 2.4 | 2.78 | 0.0 | 2.9 |
| | | Pd | Pd-O | 1.3 | 2.04 | 1.0 | 0.6 |
| | | | Pd-Pd | 1.5 | 2.75 | 1.0 | −3.9 |
| | | | Pd-Au | 7.3 | 2.78 | 1.0 | −6.0 |
| | 5 min | Au | Au-Au | 8.8 | 2.85 | 0.0 | −0.3 |
| | | | Au-Pd | 2.4 | 2.78 | 0.0 | 3.1 |
| | | Pd | Pd-O | 1.2 | 2.05 | 1.0 | 4.0 |
| | | | Pd-Pd | 1.3 | 2.75 | 1.0 | −3.6 |
| | | | Pd-Au | 6.2 | 2.78 | 1.0 | −5.8 |
| 300 sc% Pd-on-Au/C | Baseline | Au | Au-Au | 8.6 | 2.85 | 0.0 | −0.6 |
| | | | Au-Pd | 2.4 | 2.78 | 0.0 | 4.8 |
| | | Pd | Pd-O | 2.6 | 2.04 | 1.0 | −1.3 |
| | | | Pd-Pd | 1.1 | 2.75 | 1.0 | 2.0 |
| | | | Pd-Au | 2.3 | 2.78 | 1.0 | −2.5 |
| | 5 min | Au | Au-Au | 9.1 | 2.85 | 0.0 | 0.1 |
| | | | Au-Pd | 2.2 | 2.78 | 0.0 | 3.5 |
| | | Pd | Pd-O | 1.2 | 2.05 | 1.0 | −0.6 |
| | | | Pd-Pd | 4.5 | 2.75 | 1.0 | −1.7 |
| | | | Pd-Au | 4.9 | 2.78 | 1.0 | −2.8 |

increasingly larger 2-D and 3-D Pd ensembles (Pd-Pd of 1.5 and 1.1, and Pd-O of 1.3 and 2.6 for the 150 sc% and 300 sc% respectively (Table 2) compared to the 60 sc% Pd-on-Au/C. The overall degree of oxidation increased with the increase in Pd; the 150 sc% and 300 sc% had 38% and 65% of the Pd oxidized, which is expected given the stabilizing effect of Au on Pd. In comparison, the commercial monometallic Pd/C was ~60% oxidized. Treating the catalysts with $H_2$ at 200 °C was sufficient to reduce all the Pd, as evidenced by the disappearance of any Pd-O in the samples. The structure of the catalysts was mostly unchanged (that is, no alloying occurred) based on the negligible changes in Au-Au, Au-Pd, and Pd-Au CN numbers before and after treatment. The Pd nanoparticle size is estimated to be 3–4 nm using the EXAFS-size relationship established in previous studies [32].

To determine what effect the reaction conditions had on the catalysts, *in situ* XAS was performed on the catalysts before reaction and after injecting the formic acid solution. Table 3 shows the results of the EXAFS fitting on the samples before reaction and at the first time point taken after adding the formic acid solution (5 min), after which no change in CNs was observed. The Au/C catalyst CN remained virtually unchanged (Table 3). Similarly, the 60 sc% Pd-on-Au/C CNs also stayed constant and the percentage of oxidized Pd stayed 20% throughout the 30 min (Fig. 3b).

The higher loaded Pd-on-Au/C showed more subtle changes during reaction. The 150 sc% Pd-on-Au/C did not have significant changes in most of its CNs (Table 3), with the exception of Pd-O, which suggests the surface structure of the catalyst was maintained. However, the percentage of oxidized Pd dropped from 37.5% to ~20% after 5 min, presumably due to reduction by either formic acid or $H_2$ generated by the formic acid reaction in situ, which was maintained through the last time point taken (30 min, Fig. 3d). The 300 sc% Pd-on-Au/C also had insignificant change in most of its coordination numbers (Table 3) but had a dramatic decrease in percentage of oxidized Pd, from 62.5% for as-synthesized sample to ~18% after 5 min (Fig. 3h).

Pd/C was similarly affected by the reaction conditions. As can be seen in Table 3 and Fig. 3g-h, the amount of Pd-O was decreased to ~10% of total Pd within the first 5 min of reaction time, and the catalyst remained reduced throughout the measurements. The Pd particle size after 5 min reaction (2–3 nm, corresponding to the measured Pd-Pd CN of 7.3; Table 2) is smaller than that seen after reduction in $H_2$ at 200 °C (3–4 nm, Pd-Pd CN of 8.6), due to the higher temperature used in the $H_2$ treatment causing the particles to sinter. The similarity between the surface Pd of the 300 sc% Pd-on-Au/C and monometallic Pd/C samples suggests that the electronic interaction between Pd and Au, in addition to the geometric effect, is important for enhanced activity and dehydrogenation selectivity for the bimetallic catalyst.

### 3.4. Pd surface structure, activity and selectivity

Tedsree and co-workers studied the structure-activity relationship of Ag-Pd core-shell NPs for formic acid decomposition, and attributed the enhanced activity (relative to monometallic Pd NPs) to electronic and geometric effects, with a TOF of 192 $h^{-1}$ observed for the most active catalyst which consisted of ~1 layer of Pd on an Ag NP core, with catalysts containing more or less Pd exhibiting lower activity [31,33,34]. The size of Pd ensembles in their catalysts was important to the chemisorption geometry of the formate species and the subsequent surface reaction pathway. Formate that chemisorbs linearly to smaller Pd ensembles and edge atoms undergo dehydration, and formate that

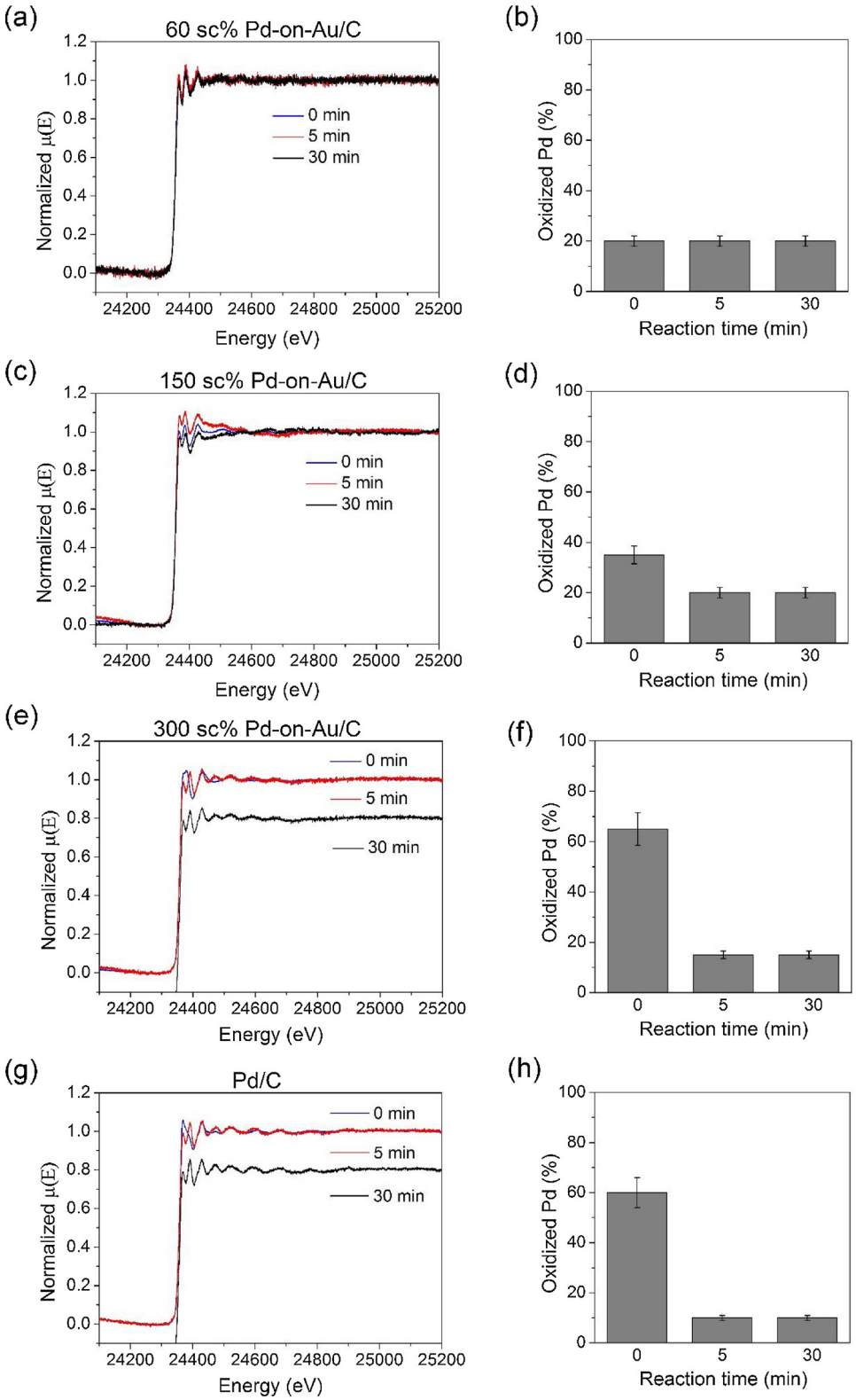


**Fig. 3.** XAS spectra at the Pd K edge and the percentage of oxidized Pd for (a, b) 60 sc% Pd-on-Au/C, (c, d) 150 sc% Pd-on-Au/C, (e, f) 300 sc% Pd-on-Au/C and (g, h) Pd/C at 0, 5 and 30 min reaction times. 30 min scan is offset in e and g for clarity.

chemisorbs in a bridging mode on larger Pd ensembles undergo the dehydrogenation pathway. Our results suggest that FA goes through a similar mechanism over the Pd-on-Au catalysts studied here (Scheme 1).

From our XAS analysis, we found the 30 sc% Pd-on-Au NPs had mostly isolated metallic Pd atoms, and generated the most CO, consistent with formate binding linearly on the small Pd ensembles, leading to the dehydration pathway. We hypothesize that the low activity observed for this catalyst was likely due to *in situ* CO poisoning of the Pd atoms. As the sc% of the Pd-on-Au NPs increases to 60 sc% and 150 sc%, we Pd ensemble size incread and decrease CO decreased, which is consistent with the hypothesis that the larger Pd ensembles

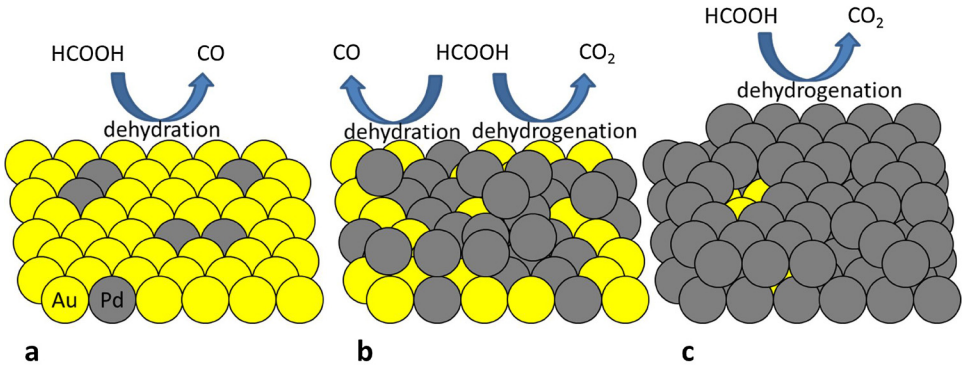


**Scheme 1.** Proposed reaction pathways on (a) low sc% Pd-on-Au NP surface, (b) intermediate sc% Pd-on-Au NP surface, and (c) high sc% Pd-on-Au NP surface.

adsorb formate in a bridging conformation and is more selective to the dehydrogenation pathway. With 300 sc%, the Pd-on-Au NPs likely have large ensembles of Pd conducive to the bridging conformation, which is reflected in the very low selectivity to CO and lack of deactivation. The fact that this catalyst, which has a surface composed primarily of Pd, is much more active than monometallic Pd catalysts suggests that the electronic effect of the Au on the Pd still has a significant role in the increased activity.

## 4. Conclusions

Pd-on-Au/C catalysts with various Pd surface coverages were studied for the room-temperature decomposition of formic acid solutions. The most active catalyst had a calculated theoretical Pd surface coverage of 300 sc% with a TOF value of 123 $h^{-1}$, much more active than monometallic Au and Pd counterparts and literature values measured in similar conditions. Pd surface coverage played an important role in the reactivity, with a catalytic activity order of 30 sc% < 60 sc% < 150 sc % < 300 sc%. The 300 sc% catalyst did not deactivate after 3 h reaction while lower sc% catalysts did. GC-TCD analysis of headspace gas indicated that the $H_2$ to $CO_2$ ratios for all catalysts were nearly 1:1, and that the CO concentration increased with decrease in Pd surface coverage. 300 sc% Pd-on-Au had no detectable amount of CO while 30 sc% one had the highest. *In situ* XAFS analysis showed that oxidized Pd was partially reduced for 150 and 300 sc% Pd-on-Au and Pd/C, while the core-shell structures of all Pd-on-Au catalysts were preserved. Electronic effects (i.e. Au stabilizing Pd from oxidation) and geometric effects (i.e. the structure of surface Pd domains as well as the formation of PdAu interfacial sites) were proposed to explain the observed activity dependence on Pd surface coverage. Large 3-D Pd ensembles on 300 sc % Pd-on-Au NPs favor the dehydrogenation pathway of formic acid decomposition *via* bridging binding, while scattered Pd atoms as well as small 2-D Pd ensembles on Pd-on-Au NPs with lower surface coverages favor the dehydration pathway *via* linear binding, leading to CO formation and active site poisoning. These results give further insights into the role of Pd-ensemble size and Au electronic effects in the conversion of FA to $H_2$.

## Acknowledgments

We acknowledge financial support from the National Science Foundation (CBET-1134535), Sigma Xi Grants-in-Aid of Research (GIAR) program (G20111015157503), and Rice University. JTM was supported by the National Science Foundation under the Cooperative Agreement No. EEC-1647722. We thank use of the Advanced Photon Source was supported by the U. S. Department of Energy, Office of Science, and Office of Basic Energy Sciences (DE-AC02-06CH11357). MRCAT operations are supported by the Department of Energy and MRCAT member institutions.

## Appendix A. Supplementary data

Supplementary material related to this article can be found, in the online version, at doi:https://doi.org/10.1016/j.cattod.2018.06.044.

## References

[1] B. Loges, A. Boddien, F. Gärtner, H. Junge, M. Beller, Catalytic generation of hydrogen from formic acid and its derivatives: useful hydrogen storage materials, Top. Catal. 53 (2010) 902–914.
[2] J.D. Scholten, M.I. Qadir, V.S. Souza, Nanoparticle-catalysts for hydrogen storage based on small molecules, Recycl. Catal. 2 (2015).
[3] M. Grasemann, G. Laurenczy, Formic acid as a hydrogen source–recent developments and future trends, Energy Environ. Sci. 5 (2012) 8171–8181.
[4] S. Enthaler, J. von Langermann, T. Schmidt, Carbon dioxide and formic acid—the couple for environmental-friendly hydrogen storage? Energy Environ. Sci. 3 (2010) 1207.
[5] M. Ojeda, E. Iglesia, Formic acid dehydrogenation on Au-based catalysts at near-ambient temperatures, Angew. Chem. Int. Ed. 48 (2009) 4800–4803.
[6] D.A. Bulushev, S. Beloshapkin, J.R.H. Ross, Hydrogen from formic acid decomposition over Pd and Au catalysts, Catal. Today 154 (2010) 7–12.
[7] Y. Huang, X. Zhou, M. Yin, C. Liu, W. Xing, Novel PdAu@Au/C core−shell catalyst: superior activity and selectivity in formic acid decomposition for hydrogen generation, Chem. Mater. 22 (2010) 5122–5128.
[8] X. Zhou, Y. Huang, C. Liu, J. Liao, T. Lu, W. Xing, Available hydrogen from formic acid decomposed by rare earth elements promoted Pd-Au/C catalysts at low temperature, ChemSusChem 3 (2010) 1379–1382.
[9] Ö. Metin, X. Sun, S. Sun, Monodisperse gold–palladium alloy nanoparticles and their composition-controlled catalysis in formic acid dehydrogenation under mild conditions, Nanoscale 5 (2013) 910–912.
[10] Z.-L. Wang, J.-M. Yan, H.-L. Wang, Y. Ping, Q. Jiang, Au@ Pd core–shell nanoclusters growing on nitrogen-doped mildly reduced graphene oxide with enhanced catalytic performance for hydrogen generation from formic acid, J. Mater. Chem. A 1 (2013) 12721–12725.
[11] W.-Y. Yu, G.M. Mullen, D.W. Flaherty, C.B. Mullins, Selective hydrogen production from formic acid decomposition on Pd–Au bimetallic surfaces, J. Am. Chem. Soc. 136 (2014) 11070–11078.
[12] M.O. Nutt, J.B. Hughes, M.S. Wong, Designing Pd-on-Au bimetallic nanoparticle catalysts for trichloroethene hydrodechlorination, Environ. Sci. Technol. 39 (2005) 1346–1353.
[13] M.O. Nutt, K.N. Heck, P.J.J. Alvarez, M.S. Wong, Improved Pd-on-Au bimetallic nanoparticle catalysts for aqueous-phase trichloroethene hydrodechlorination, Appl. Catal. B 69 (2006) 115–125.
[14] K.N. Heck, M.O. Nutt, P.J.J. Alvarez, M.S. Wong, Deactivation resistance of Pd/Au nanoparticle catalysts for water-phase hydrodechlorination, J. Catal. 267 (2009) 97–104.
[15] M.S. Wong, P.J.J. Alvarez, Y.L. Fang, N. Akcin, M.O. Nutt, J.T. Miller, K.N. Heck, Cleaner water using bimetallic nanoparticle catalysts, J. Chem. Technol. Biot. 84 (2009) 158–166.
[16] Y.L. Fang, K.N. Heck, P.J.J. Alvarez, M.S. Wong, Kinetics analysis of Palladium/Gold nanoparticles as colloidal hydrodechlorination catalysts, ACS Catal. 1 (2011) 128–138.
[17] Y.L. Fang, J.T. Miller, N. Guo, K.N. Heck, P.J.J. Alvarez, M.S. Wong, Structural analysis of palladium-decorated gold nanoparticles as colloidal bimetallic catalysts, Catal. Today 160 (2011) 96–102.
[18] H.J.S.L.A. Pretzer, Y. Fang, Z. Zhao, N. Guo, T. Wu, I. Arslan, J.T. Miller, M.S. Wong, Regulating the hydrodechlorination activity of Pd-on-Au nanoparticles with Au particle size, J. Am. Chem. Soc. (2012) submitted.
[19] J.C. Velázquez, S. Leekumjorn, Q.X. Nguyen, Y.-L. Fang, K.N. Heck, G.D. Hopkins, M. Reinhard, M.S. Wong, Chloroform hydrodechlorination behavior of alumina-supported Pd and PdAu catalysts, Aiche J. 59 (2013) 4474–4482.
[20] H. Qian, Z. Zhao, J.C. Velazquez, L.A. Pretzer, K.N. Heck, M.S. Wong, Supporting palladium metal on gold nanoparticles improves its catalysis for nitrite reduction,

Nanoscale 6 (2014) 358–364.
[21] L.A. Pretzer, K.N. Heck, S.S. Kim, Y.-L. Fang, Z. Zhao, N. Guo, T. Wu, J.T. Miller, M.S. Wong, Improving gold catalysis of nitroarene reduction with surface Pd, Catal. Today 264 (2016) 31–36.
[22] Z. Zhao, J. Arentz, L.A. Pretzer, P. Limpornpipat, J.M. Clomburg, R. Gonzalez, N.M. Schweitzer, T. Wu, J.T. Miller, M.S. Wong, Volcano-shape glycerol oxidation activity of palladium-decorated gold nanoparticles, Chem. Sci. 5 (2014) 3715–3728.
[23] Z. Zhao, J. Miller, T. Wu, N. Schweitzer, M. Wong, EXAFS characterization of palladium-on-gold catalysts before and after glycerol oxidation, Top. Catal. 58 (2015) 302–313.
[24] M.O. Nutt, K.N. Heck, et al., Improved Pd-on-Au bimetallic nanoparticle catalysts for aqueous-phase trichloroethene hydrodechlorination, Appl. Catal. B-Environ. 69 (2006) 115–125.
[25] Y.-L.F.Z. Zhao, P.J.J. Alvarez, M.S. Wong, Degrading perchloroethene at ambient conditions using Pd and Pd-on-Au reduction catalysts, Appl. Catal. B-Environ. 140-141 (2013) 468–477.
[26] L.A. Pretzer, H.J. Song, Y.-L. Fang, Z. Zhao, N. Guo, T. Wu, I. Arslan, J.T. Miller, M.S. Wong, Hydrodechlorination catalysis of Pd-on-Au nanoparticles varies with particle size, J. Catal. 298 (2013) 206–217.
[27] Z. Zhao, J. Arentz, L.A. Pretzer, P. Limpornpipat, J.M. Clomburg, R. Gonzalez, N. Schweitzer, T. Wu, J.T. Miller, M.S. Wong, Tuning the catalytic activity and selectivity of palladium-decorated gold for glycerol oxidation, J. Am. Soc. Chem. (2013) to be submitted.
[28] A. Mailhe, P. Sabatier, Catalytic decomposition of formic acid, Comp. Rend. Acad. Sci. 152 (1911) 1212–1215.
[29] O. Deutschmann, H. Knözinger, K. Kochloefl, T. Turek, Heterogeneous Catalysis and Solid Catalysts, Ullmann's Encyclopedia of Industrial Chemistry, Wiley-VCH Verlag GmbH & Co. KGaA, 2000.
[30] Q.-Y. Bi, X.-L. Du, Y.-M. Liu, Y. Cao, H.-Y. He, K.-N. Fan, Efficient subnanometric gold-catalyzed hydrogen generation via formic acid decomposition under ambient conditions, J. Am. Chem. Soc. 134 (2012) 8926–8933.
[31] K. Tedsree, T. Li, S. Jones, C.W.A. Chan, K.M.K. Yu, P.A.J. Bagot, E.A. Marquis, G.D.W. Smith, S.C.E. Tsang, Hydrogen production from formic acid decomposition at room temperature using a Ag-Pd core-shell nanocatalyst, Nat. Nano 6 (2011) 302–307.
[32] J.T. Miller, A.J. Kropf, Y. Zha, J.R. Regalbuto, L. Delannoy, C. Louis, E. Bus, J.A. van Bokhoven, The effect of gold particle size on AuAu bond length and reactivity toward oxygen in supported catalysts, J. Catal. 240 (2006) 222–234.
[33] K.S. Kim, M.A. Barteau, Structural dependence of the selectivity of formic acid decomposition on faceted titania (001) surfaces, Langmuir 6 (1990) 1485–1488.
[34] N. Hoshi, M. Nakamura, K. Kida, Structural effects on the oxidation of formic acid on the high index planes of palladium, Electrochem. Commun. 9 (2007) 279–282.